Synthesis of Antimicrobial and Antioxidant Zinc Oxide Hydrogel for Drug Delivery Applications

Krithika Ramesh[1*], Jeyanthi Ponnusamy[2], and Pazhanisamy Periasamy[3]

[1]*Department of Chemistry, Bharathiyar University, Maruthamalai Road, Coimbatore 641046, India*

[2]*Department of Chemistry, Queen Mary's College, Dr. Radha Krishna Salai, Chennai 600004, India*

[3]*Department of Chemistry, Sir Theagaraya College, 1047, Thiruvottiyur High Rd, Chennai-600021, India*

**** Corresponding author:***

email: krithikaramesh@hotmail.com

Received: June 13, 2023
Accepted: August 11, 2024

DOI: 10.22146/ijc.85663

Abstract: *A novel and simple method was used to synthesize antimicrobial and antioxidant porous (*N-tert-*butylacrylamide-co-*N-*vinylpyrrolidone) zinc oxide hydrogel via free radical copolymerization. The hydrogel was characterized by NMR, XRD, and SEM. Thermodynamic properties of the hydrogel were described quantitatively by the Flory-Rehner method. The results indicate that the synthesized hydrogel exhibits strong antioxidant activity, making it a potential candidate for use in preventing degenerative diseases. The antimicrobial tests showed that the hydrogel could inhibit the growth of Gram-positive and Gram-negative bacteria, as well as some pathogenic bacteria and fungi. The inhibition zones ranged from 10 to 15 mm for bacteria and from 5.2 to 9.1 mm for fungi. The reactivity ratio $r_1 \times r_2$ equal to 1 confirmed ideal copolymerization showed the composition of the copolymer and the comonomer feed are same. The hydrogel's structure and reactivity are significant for constructing effective delivery systems for specific applications. Optimizing the monomer proportion could enhance hydrogel efficiency and release behavior. The hydrogel's water solubility, non-toxicity, and antioxidant properties suggest it could be safe and effective throughout the drug delivery process, contributing both passive and reactive targeting functions.*

Keywords: *polymeric gel; free-radical copolymerization; drug loading; antimicrobial; antioxidant property*

■ INTRODUCTION

The integration of advanced materials in biomedical applications has experienced remarkable growth, particularly through the innovative use of hydrogels and nanomaterials. Bhandari et al. [1] discuss the synthesis and characterization of zinc oxide nanoparticles, emphasizing their transformative potential in enhancing drug delivery systems. Hydrogels, especially spherical variants, have garnered extensive research attention for their swelling behaviors and drug release capabilities, as previously illustrated [2-3]. The adaptability of biodegradable polymers in medical applications highlights a shift towards more sustainable solutions [4]. Recent developments in starch-based hydrogels using a double-network method showcase their promise in biomedical applications, including tissue engineering [5]. Insights into the latest trends in biomaterials and nanomaterials are provided by Fenton et al. [6] and Ibrahim et al. [7], respectively, underscoring their critical roles in advancing modern biomedicine. Furthermore, the investigation of vapor pressure and interaction parameters in polymeric solutions also enhances our understanding of swelling and functional properties [8-9].

van der Sman [10] applied scaling laws and Flory-Rehner theory to analyze biopolymer gel swelling, while Sen et al. [11] examined the molecular weight between cross-links in diprotic acid-containing hydrogels. Alidoust et al. [12] investigated the adsorption of free radical TEMPO onto Al_2O_3 nanoparticles, shedding light on radical scavenging activities that enhance drug

stability and efficacy. The study of radical copolymerization reactivity ratios highlights essential insights into polymer behavior [13]. The reactivity ratios relevant to copolymerization processes are crucial for designing tailored drug-loaded nanoparticles [14-15]. Additionally, Yu and Xing [16] examined moisture absorption in carbon fiber-reinforced polymers, underscoring the significance of understanding Fickian and non-Fickian diffusion in crafting effective drug delivery systems. Zhokh and Strizhak [17] further illustrated the intricate interplay of drug release mechanisms and diffusion processes in colloidal systems.

Electrospun bioscaffolds incorporating cellulose acetate and dendrimer-modified cellulose nanocrystals presents promising avenues for controlled drug release [18]. Injectable hydrogels composed of collagen, chitosan, and hyaluronic acid have demonstrated considerable potential in tissue engineering [19]. The radical scavenging activities of silver nanoparticles synthesized using natural materials offer additional strategies for enhancing therapeutic effectiveness [20]. Recent developments in stimuli-responsive hydrogels alongside investigations into poly(*N*-isopropylacrylamide) hydrogels for wound dressing applications highlight the expanding versatility of hydrogels in biomedical settings [21-22]. Cross-linked hyaluronic acid hydrogel films were developed by Luo et al. [23]. Research into drug-loaded hydrogels designed for sustained release by Thippeswamy et al. [24] and Naeem et al. [25] represents cutting-edge efforts to optimize drug delivery systems for improved patient outcomes.

This study aims to synthesize porous zinc oxide (*N*-*tert*-butylacrylamide-co-*N*-vinylpyrrolidone) hydrogel through free-radical polymerization and to study its bio-protective properties. Applications are not limited for drug targeting, controlled drug release, and stabilizing labile molecules. No previous studies were reported on the synthesis of hydrogel using zinc oxide.

■ EXPERIMENTAL SECTION

Materials

Acrylamide (AM), procured from Merck was crystallized from acetone/ethanol mixture, *N*-vinylpyrrolidone (NVP) was obtained from Merck, and 2,2'-azobis(isobutyronitrile) (AIBN) from Merck was crystallized twice from methanol. The crosslinker *N*,*N*'-methylene-bis-acrylamide (MBA) from Merck was used as received, methanol from Sigma Aldrich, and distilled water from Millipore system implanted in the lab. For the antimicrobial activity test, *Escherichia coli* (ATCC 25922) and αDH5 strain, as well as *Trichophyton rubrum* were used in this research.

Instrumentation

The morphology and porous structure of hydrogel were examined using a scanning electron microscope with EDS system (SEM EDAX XL30) and X-ray diffractometer, Shimadzu, Japan, with X-ray Tube Cu Kα with a wavelength of 1.54060 Å, under continuous scanning mode with a speed range of 2θ.

Procedure

Synthesis of porous zinc oxide hydrogel

Acrylonitrile (20 g) was first washed with 100 mL of 5% NaOH solution in water to remove the inhibitor and then washed with 100 mL of 3% orthophosphoric acid solution in water to remove basic impurities. The acrylonitrile was then washed with twice the amount of distilled water and dried in an anhydrous solution of $CaCl_2$. The acrylonitrile was then distilled in an atmosphere of nitrogen and reduced pressure. It was then collected in a clean amber-colored bottle and kept in the refrigerator at 50 °C. The monomers *N*-*tert*-butylacrylamide (NTB) were prepared by reacting *tert*-butyl alcohol with acrylonitrile. NTB was recrystallized in dry benzene [14-15].

The reactant monomers, consisting of 0.5 g of NTB, 0.5 g of NVP, and varying amounts of the crosslinker MBA (0.05, 0.025, and 0.075 g for three different proportions), were dissolved in 20 mL of a water-methanol solvent mixture in a 3:1 ratio, respectively. AIBN is more soluble in water-methanol solvent than in water (solubility 0.1). MBA, a cross-linker, forms crosslinks by polymerizing with acrylamide within the gel by increasing firmness [7]. The reactant monomer mixtures were prepared at different proportions by adding NTB, NVP, MBA (0.025, 0.050, and 0.075 g in 2 mL water), 0.05 g of AIBN and 0.01 g of zinc oxide nano

Table 1. Variable amount of crosslinker used for the synthesis of porous ZnO hydrogel in methanol:water (3:1)

Sample	Weight (g)			
	NTB	NVP	MBA	ZnO
1	0.5	0.5	0.050	0.01
2	0.5	0.5	0.025	0.01
3	0.5	0.5	0.075	0.01

powder refer to Table 1. The reactant mixture was stirred constantly for 30 min. The mixed contents were placed in a polymerization tube and flushed with nitrogen gas for about 30 min. The polymerization tube was closed with a rubber cork and kept in a thermostat water bath maintained at 60 °C centigrade. After 12 h, the reaction mixture was tested for reaction completion and poured into ice-cold water. The precipitated polymer gel was washed with benzene to remove unreacted monomer, dried air, and vacuum. Then, it is cut into pieces of similar size of approximately 2 mm [21].

Porosity

The solvent replacement method was employed to measure the porosity of the hydrogel. After immersing the hydrogel in ethanol for a night, it was dried to remove excess ethanol and weighed. The porosity of the hydrogel was measured by Eq. (1);

$$\text{Porosity} = \frac{M_2 - M_1}{\rho V} \times 100 \quad (1)$$

M_1 is the mass of the dried hydrogel, M_2 is the mass of the dried hydrogel after ethanol immersion, V is the hydrogel volume, and ρ is the ethanol density [5].

Swelling characteristics

The swelling characteristics of the hydrogel were measured using double distilled water. During each experiment, a known weight of the dried hydrogel sample was immersed in double distilled water, and swelling measurements were recorded. The swelling ratio of the hydrogel is evaluated by Eq. (2);

$$\text{Swelling ratio (Q)} = \frac{M_s - M_d}{M_d} \quad (2)$$

Q is the swelling ratio, M_s is the mass of the hydrogel in the swollen state, and M_d is the mass of the dried hydrogel [2].

Structural analysis of hydrogel

Hydrogels are largely dependent on gel performance or their bulk structure for drug delivery. The network structure of hydrogel was determined by using the following parameters. The diffusion coefficient was measured by the rate of the diffusing substances transported in a cubic system between the opposite faces depending on polymer segment progress, which is calculated by Eq. (3);

$$D = \pi \left(\frac{h \times \theta}{4 \times q_{eq}} \right)^2 \quad (3)$$

q_{eq} is the value of the swollen gel at equilibrium, θ is the slope of the swollen curves linear portion, and h is the thickness of the gel at the initial state before swelling [25].

The M_c denoted the amount of crosslinking of the hydrogel system between the two adjacent crosslinks and described the addition of polymer and liquid. The Flory-Rehner in Eq. (4) was used to calculate the M_c value;

$$M_c = -\frac{d_p V_s \left(V_{2,S}^{1/3} - \frac{V_{2,S}}{2} \right)}{\ln\left(1 - V_{2,S}\right) + V_{2,S} + \chi V_{2,S}^{\ 2}} \quad (4)$$

where d_p is the density of polymer, V_s is the solvent molar volume, and χ is the Flory interaction parameter of polymer-solvent [25]. Then, $V_{2,S}$ is calculated in Eq. (5);

$$V_{2,S} = \left(1 + \frac{d_p}{d_s} \left(\frac{M_a}{M_b} - 1 \right) \right)^{-1} \quad (5)$$

where d_s is the density of the solvent. M_a and M_b are the mass of the hydrogel and dry and swollen state, respectively. $V_{2,S}$ is the volume fraction of the gel in the swollen state [25]. Then, χ is calculated using Eq. (6);

$$\chi = \frac{\ln\left(1 - V_{2,S}\right) + V_{2,S}}{V_{2,S}} \quad (6)$$

N is calculated from the value of the average molecular weight between cross-links [25] derived from Eq. (7);

$$N = \frac{M_c}{M_r} \quad (7)$$

N is the number of links between two crosslinks, M_c is calculated from the average molecular weight of crosslinks, and M_r is the molar mass of the repeating unit [25] given by Eq. (8);

$$M_r = \frac{m_{NTB}M_{NTB} + m_{NVP}M_{NVP} + m_{MBA}M_{MBA}}{m_{NTB} + m_{NVP} + m_{MBA}} \quad (8)$$

where m_{NTB}, m_{NVP}, and m_{MBA} are the masses of NTB, NVP, and MBA, respectively. Then, M_{NTB}, M_{NVP}, and M_{MBA} are the molar masses of NTB, NVP, and MBA, respectively [25].

Drug loading and release

Loading of drugs is the efficiency of the research method to incorporate a drug into the carrier system. Drug release could be explained as a process of migration of drug from the initial position to the outer surface and finally to a polymeric system of the release medium [6]. The absorbance spectra of chloramphenicol were used to measure its concentration. The maximum absorbance of chloramphenicol is directly proportional to its concentration. The volume of the drug solution was calculated as 100 times the dried hydrogel's weight. The estimated amount of drug released from the hydrogel is determined by measuring the spectra of the release medium at constant time intervals [3,18].

Chloramphenicol was prepared in 50 mL of 100 ppm (drug) and dissolved in 50 mL of PBS buffer solution by stirring for 30 min. Prepared gels were extracted, dried, and weighed. The known weight of dried hydrogels was added to clean three glass vials and labeled as 1D, 2D, and 3D. Chloramphenicol in PBS buffer solution was added to the hydrogel and kept in glass vials. Then, it was closed and stored away from direct sunlight. Drug release was measured by setting the baseline wavelength of 290–300 nm in the UV-vis spectrophotometer using the PBS buffer solution. The absorbance of the chloramphenicol was measured at 272 nm. Soaked hydrogels were removed from the glass vials, transferred to another set of 3 glass vials (1a, 2a, and 3a) of known PBS buffer solution, and stored. The absorbance of the solution is measured at different intervals of time [18,22].

Protein loading and release

Bovine serum albumin (BSA) of 0.005 g (protein) was prepared in 50 mL of the PBS buffer solution by constantly stirring for 30 min. Prepared gels were dried and weighed. The known weight of dried hydrogels was added, cleaned, and wiped, and three glass vials were labeled 1P, 2P, and 3P. BSA solution was added to the glass vials, which were closed and stored away from direct sunlight. Protein release was measured by setting the baseline wavelength (290–300 nm) in the UV-vis spectrophotometer using the buffer PBS solution. The absorbance of the BSA was measured at 280 nm. Soaked hydrogels were removed from the glass vials and transferred to another set of 3 glass vials (1a, 2a, and 3a) of known volume of PBS buffer solution and stored. The absorbance of the solution was measured at different intervals of time.

Evaluation of free radical scavenging activity of hydrogel

The scavenging activity of the hydrogel was evaluated by employing the 2,2-diphenyl-1-picrylhydrazyl (DPPH) method. First, 2.9 mg of DPPH was dissolved in 100 mL methanol and incubated in the dark for 24 h at 20 °C. Then, 10 mL of DPPH solution was taken from the stock solution and diluted with methanol, and absorbance was measured at 517 nm. An aliquot of each dilution was mixed with DPPH in methanol. The IC_{50} is a fundamental concept of pharmacology and is calculated using response variables and growth inhibition data. The concentration of the sample required to decrease the concentration of the DPPH by 50% was calculated using linear regression analysis and calculated using Eq. (9) [20];

$$IC_{50} = \frac{0.5 - b}{a} \quad (9)$$

where a and b are the slope and intercept, respectively. The inhibition activity was calculated by the following Eq. (10);

$$\%\text{Scavenging} = \frac{Abs_{control} - Abs_{sample}}{Abs_{control}} \times 100\% \quad (10)$$

$Abs_{control}$ and Abs_{sample} are the absorbance of the control and sample, respectively [12].

Antimicrobial analysis

An antimicrobial study was conducted using the standard agar well diffusion method. In brain heart infusion broth, bacteria, and fungi were isolated and diluted to 10^5 colony-forming units approximately per mL. Then, 5 mm diameter wells were cut and filled with 30 µL of the sample solution using a sterile cork borer. The plates were incubated for 18 h at 37 °C for bacteria. Similarly, the plates were incubated for 18 h at room temperature for fungi.

■ RESULTS AND DISCUSSION

Synthesis and Characterization

This work aimed to synthesize a porous *N*-tert-butylacrylamide-co-*N*-vinylpyrrolidone-zinc oxide hydrogel by free-radical polymerization. The monomers are NTB, NVP, MBA as the crosslinker, and AIBN as the polymerization initiator. While the free-radical polymerization reaction was initiated, the dissociated radicals of AIBN attacked the double bonds of NTB, NVP, and MBA. When the double bond was cleaved, a covalent bond between the monomers formed a long aliphatic chain, which was then attached by the crosslinker added consecutively.

The ^{1}H-NMR spectra of the monomers and copolymers showed the following peaks in the NTB spectrum: *tert*-butyl proton at 1.42 ppm, vinyl proton at 5.59–6.28 ppm, and N–H proton at 7.27 ppm. SEM/EDAX images revealed that the zinc oxide nanoparticles were spherical and uniformly distributed throughout the polymer matrix. SEM/EDAX microanalysis was used to determine the composition of the zinc oxide nanoparticles within the hydrogel matrix. Surface and cross-sectional micrographs confirmed the presence of zinc oxide nanoparticles in the hydrogel polymer matrix through EDAX analysis, with the representative EDAX spectrum showing well-resolved peaks for zinc, carbon, and oxygen.

Monomer and copolymer composition of NTB and NVP in the feed and polymer was calculated and shown in Table 2. In the maximum cross-linker concentration of 0.025 g, the porosity percentage increased to 18.5%. With a diffusion exponent of 0.62, the swelling rate increased with increasing pH. The loading and release behavior showed a substantial increase in the loading and release efficiency of the drug in the hydrogels, exhibiting significant antibacterial and antifungal activities. The copolymerization behavior of monomer and copolymer is given in Fig. 1.

Hydrogel Characterization

The ^{1}H-NMR spectra of copolymers were recorded on the GSX-400 spectrometer (JEOL, Tokyo, Japan) operating at 400 MHz in $CDCl_3$. The ^{1}H-NMR revealed distinct peaks between 1.1 and 1.4 ppm are characteristic of *tert*-butyl protons, which produce a singlet due to the equivalent and symmetrical nature of the three methyl groups attached to a central carbon ($-C(CH_3)_3$) in Fig. S1. The peaks at 2.8, 2.2, and 1.5 ppm correspond to the methylene protons of the NVP ring. Specifically, the peaks at 2.8 and 2.2 ppm correspond to the methylene groups adjacent to the nitrogen atom in the pyrrolidone ring, indicating the presence of these functional groups and their chemical environment in the molecule. The peak at 1.5 ppm corresponds to the methylene protons further from the nitrogen, experiencing less electron-withdrawing influence. These shifts highlight the unique

Table 2. Monomer and copolymer composition

Sample	Mole fraction in the feed		Monomer in polymer	
	NTB (M_1)	NVP (M_2)	NTB (m_1)	NVP (m_2)
1	0.3	0.7	0.3577	1.0050
2	0.4	0.6	0.4411	0.7643
3	0.5	0.5	0.6150	0.9553
4	0.6	0.4	0.6473	0.8619
5	0.7	0.3	0.7373	0.5732

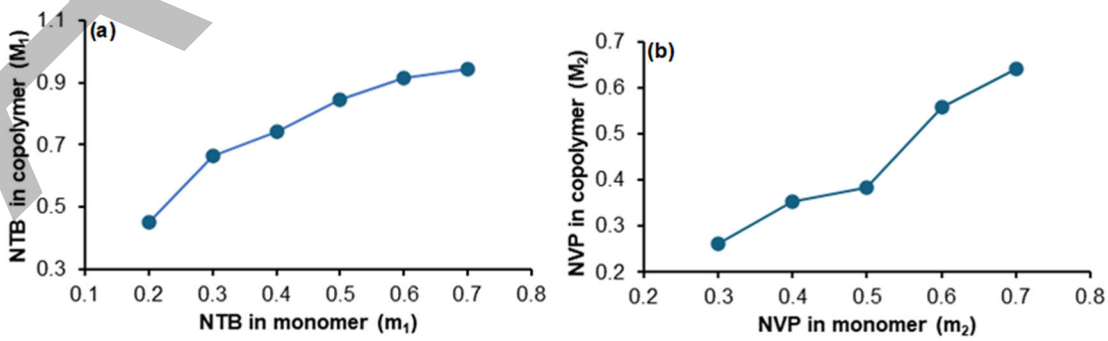

Fig 1. Monomer and copolymer composition of (a) NTB and (b) NVP

electronic environments and provide structural information significant for characterizing the hydrogel molecular framework.

Fig. 2(a-c) revealed the hydrogel's uniform shape and particle distributions. The surface contains many pores connected. The capillary networks are clearly detected from the SEM image, and this could enable water to enter the hydrogel networks or drug molecules to diffuse out of them. The synthesized hydrogel's EDAX spectrum showed well-resolved zinc, carbon, nitrogen, and oxygen peaks.

The Fineman-Ross equation is utilized to analyze the relationship between the composition of a copolymer and the feed mixture. This equation states how the feed composition influences the copolymer's final composition [14]. F represents the ratio of M_1 to M_2 in the feed, and this ratio provides insight into the initial feed composition [16]. The ratio of m_1 to m_2 in the copolymer is denoted by f, and this ratio reflects the composition of the resulting copolymer. The deviation of the copolymer composition from the feed composition is given by (f-1), indicating the difference of copolymer's mole fraction of m_1 from 1, highlighting how the copolymer composition deviates from a specific reference [14].

The Kelen-Tüdős parameters are crucial for analyzing the composition and properties of copolymers such as poly(*N*-tert-butylacrylamide-co-*N*-vinylpyrrolidone). These parameters reveal how the feed composition affects the final structure of the copolymer. The parameter G indicates how the copolymer's composition deviates from the feed composition. H captures the scaling effect of the feed composition on the copolymer. The G and H are calculated in Eq. (11) and (12), respectively [14].

$$G = \frac{F(f-1)}{f} \tag{11}$$

$$H = \frac{F^2}{f} \tag{12}$$

The normalization factor α helps balance the effects of G and H. Data points provide insights into how variations in feed composition influence the copolymer properties. At the same time, the parameters η and ξ reveal the combined effects of deviation and scaling on the copolymer structure. The η and ξ are calculated in Eq. (13) and (14), respectively.

$$\eta = \frac{G}{\alpha + H} \tag{13}$$

$$\xi = \frac{H}{\alpha + H} \tag{14}$$

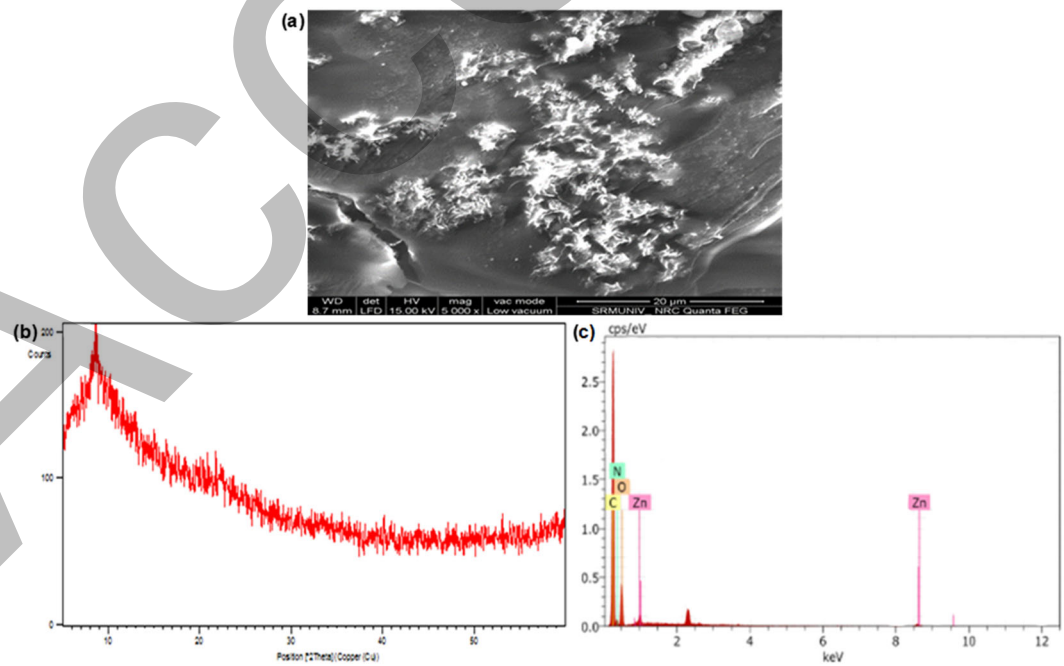

Fig 2. (a) SEM, (b) XRD pattern, and (c) EDAX spectra of (*N*-tert-butylacrylamide–co-*N*-vinylpyrrolidone) zinc oxide hydrogel

Additionally, ratios r_1 and r_2 serve as further adjustment factors, highlighting the relative impact of feed composition on the copolymer characteristics [14].

Tables 3 and 4 show the Fineman-Ross and Kelen-Tüdős parameters. G values range from −0.3409 to 1.5019, indicating a variable reactivity of the monomers. The negative G values at lower mole fractions suggest less favorable polymerization conditions, while positive G values at higher mole fractions indicate more favorable conditions. The H values, ranging from 0.3298 to 1.9398, increase with the mole fraction, reflecting a growing impact of f parameter on the reactivity ratios and polymerization process. For η, the values span from −0.09651 to 3.8176, illustrating how the combination of G and H (influenced by α) affects the copolymerization behavior. Similarly, ξ values range from 0.7421 to 4.3651, demonstrating how the ratio of H to α influences the overall copolymer characteristics. Together, these parameters help in understanding how the reactivity of the monomers and their proportions impact the formation and properties of the copolymer.

Reactivity ratios were evaluated using the Fineman-Ross and Kelen-Tüdős models. In the Fineman-Ross method, plotting G and H variables yields a straight line where the gradient represents r_1 and the intercept represents r_2. G and H are derived from the mole fractions of the monomers in the feed and the resulting copolymer. The Kelen-Tüdős model enhances this approach by introducing an arbitrary constant (α) to correct for data bias and improve the uniformity of the data. This adjustment transforms G and H into new variables ξ and η. The reactivity ratios were then determined from ξ and η. The values H_{min} and H_{max} represent the minimum and maximum values of the derived H. The efficiency of copolymerization is shown in Tables 3 and 4. The r_1 and r_2 reactivity ratios were 1, indicating ideal conditions for polymerization determined in Table 5.

Fig 3(a) shows the Fineman-Ross plot, which illustrates the relationship between the feed composition and the copolymer composition, providing insights into how variations in the feed ratio affect the copolymer's structure. Fig 3(b) displays the Kelen-Tüdős plot, which visualizes the Kelen-Tüdős parameters and their impact on the copolymer composition, highlighting the influence

Table 3. Fineman–Ross parameters of poly(*N*-tert-butylacrylamide-co-*N*-vinylpyrrolidone)

F	f	f-1
0.4285	0.5569	−0.4430
0.6666	0.7892	−0.2107
1.0000	1.5974	0.5974
1.5000	1.8352	0.8352
2.3333	2.8066	1.8066

Table 4. Kelen-Tüdős parameters for the copolymers of poly(*N*-tert-butylacrylamide-co-*N*-vinylpyrrolidone)

G	H	η	ξ
−0.3409	0.3298	−0.0965	0.7421
−0.1780	0.5631	0.3405	1.2672
0.3739	0.6260	1.0935	1.4086
0.6826	1.2259	2.0795	2.7587
1.5019	1.9398	3.8176	4.3651

Table 5. Reactivity ratios of *N*-tert-butylacrylamide and *N*-vinylpyrrolidone

Parameters	r_1	r_2	r_1r_2
Fineman-Ross	0.9769	1.0546	1.0302

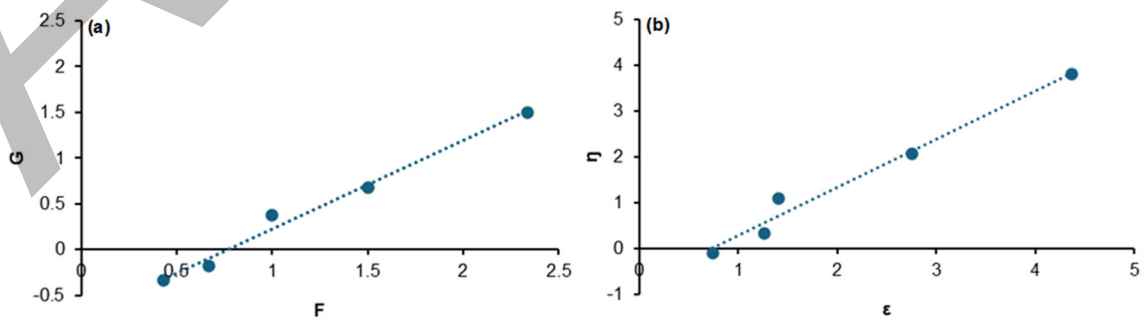

Fig 3. (a) Fineman-Ross and (b) Kelen-Tüdős plots

Table 6. Mean sequence length of poly(*N*-tert-butylacrylamide-co-*N*-vinylpyrrolidone)

Mole fraction of NVP in feed (M_2)	μNTB (l_1)	μNVP (l_2)	l_1:l_2	Distribution*
0.7	1.4148	2.7259	1:3	BVVVVB
0.6	1.8752	2.1095	2:2	BBVVBB
0.5	1.9679	1.7937	2:2	BBVVBB
0.4	2.4618	1.4931	2:1	BBVBB
0.3	3.2584	1.3170	3:1	BBBVBBB

**N*-tert-butylacrylamide represented as B; *N*-vinylpyrrolidone represented as V

of feed composition on the resulting copolymer properties.

The μNTB and μNVP mean sequence lengths were computed and tabulated using the following Eq. (15) and (16) and shown in Table 6 [14].

$$\mu NTB = r_1\left(\frac{M_1}{M_2}\right)+1 \quad (15)$$

$$\mu NVB = r_2\left(\frac{M_2}{M_1}\right)+1 \quad (16)$$

μNVP value increases in the copolymer NTB/NVP with the rise in the concentration of NVP in the feed. The copolymer is enriched with NVP monomer concentration, obtained from the values r_1 of 0.9769 and r_2 of 0.7397.

Porosity Measurement

Porosities of porous hydrogels indicated a decrease in porosity with increased MBA concentration. An increase in the concentration of MBA yielded an increase in the degree of polymer chain branching and a decrease in the network area, as shown in Table 7.

Swelling Studies and Effect of MBA Concentration

The porous hydrogel showed a decrease in swelling capacity with an increase in MBA concentration, referring to Fig. 4. The data revealed that the ability of the porous hydrogel to swell depended on the medium's pH [22]. The porous hydrogel, swollen in water, exhibited a very short swelling time to reach its equilibrium size, referred to in Fig. 5. Crosslinkers play a major role in preventing hydrophilic polymer chains from dissolving in an aqueous environment [14]. In the synthesized poly(*N*-tert-butylacrylamide-co-*N*-vinylpyrrolidone) zinc oxide hydrogel, the cross-linker concentration was varied to study the effect of concentration of MBA on water absorbency and kept other reactants constant [21]. Higher concentrations of MBA showed higher density but lower porosity [14]. The cross-linker MBA concentration increased the mechanical stability but decreased the porosity through it, decreasing the diffusion rate in drug release by capillary channels [25].

Samples 1 (SP1), 2 (SP2), and 3 (SP3) are polymer samples with 0.5 g of NTB and 0.5 g of NVP. The key differences are in the MBA crosslinker and AIBN initiator amounts: SP1 has 0.025 g of MBA and 0.05 g of AIBN, SP2 has 0.05 g of MBA and 0.05 g of AIBN, and SP3 features 0.075 g of MBA with 0.05 g of AIBN. All samples include 0.01 g of ZnO. The variations in MBA concentration affect the polymer's crosslinking density and properties.

Table 7. Porosity measurement

S. No.	Weight of MBA (g)	Porosity (%)
1	0.025	18.53
2	0.050	18.39
3	0.075	18.17

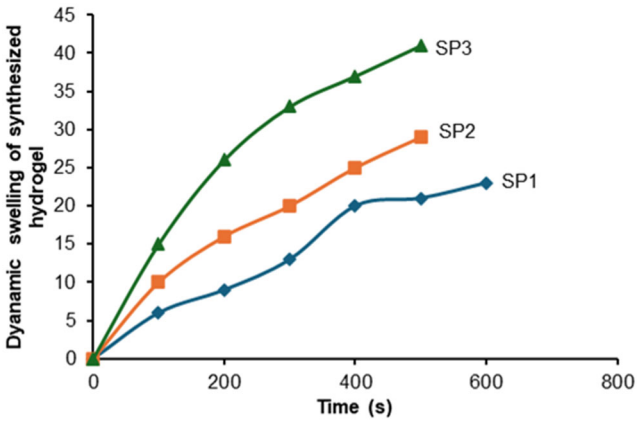

Fig 4. The effective swelling characteristics of porous hydrogel in terms of time as a function

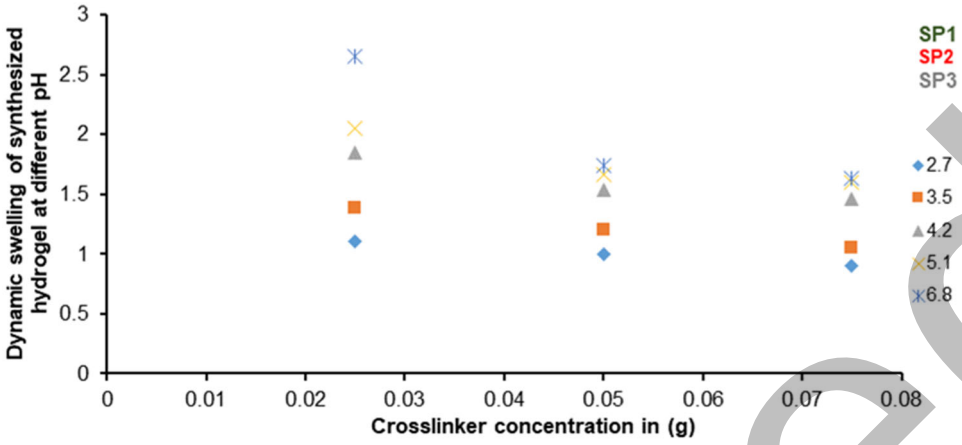

Fig 5. Effect of increasing the concentration of MBA in monomer concentration at different pH

Increasing MBA concentration enhances the polymer's crosslinking, improving its mechanical strength and stability. At various pH levels, SP1 with 0.025 g of MBA shows lower strength and flexibility, while SP2 (0.05 g) and SP3 (0.075 g) exhibit more excellent resistance to degradation and swelling, particularly at lower pH. Higher MBA concentrations in SP2 and SP3 lead to better overall stability and performance. The swelling mechanism (F_{swp}) of the samples was calculated by the Eq. (17);

$$F_{swp} = \frac{M_t - M_0}{M_0} = Kt^n \quad (17)$$

M_t, M_0, K, and n are the mass of swollen hydrogel sample, mass of the dry sample at time t, swelling constant, and swelling exponent, respectively. In cylindrical-shaped hydrogel, the value of n between 0.45–0.50 denotes the Fickian diffusion, and $0.50 < n < 1.0$ denotes the non-Fickian mechanism [25]. The swelling exponent value (n) 0.603 indicated the diffusion deviation mechanism as non-Fickian, as in Fig. 6. The plot of ln F_{swp} against ln T yielded a straight line corresponding to an increase in hydrogel mass by 60%. The slope of the plot determines the value of n.

Structural Parameters and Diffusion Coefficient of Hydrogels

The network structure of the hydrogel parameter determined the gel performance. The parameter obtained from the variation in bonded chain attraction between free volume and the solvent existed between the numbers of crosslinks (N), shown in Table 8. The Flory Polymer-solvent interaction parameter was calculated to predict the properties of the polymer solution. M_c values directly impact the physical properties of the gel, as it is directly proportional to tensile strength and glass transition temperature.

Drug Loading and Release

The result data inferred that the drug is released constantly in a lower pH solution than in a higher pH.

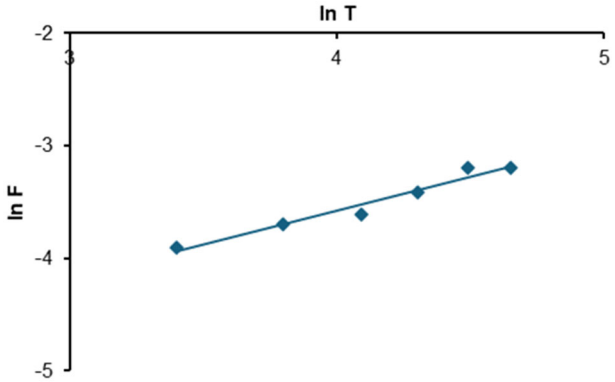

Fig 6. Swelling kinetics curves of (*N*-tert-butylacrylamide-co-*N*-vinylpyrrolidone) zinc oxide hydrogel crosslinked by MBA

Table 8. Diffusion coefficient of hydrogels

Sample	$V_{2,s}$	χ	M_c	M_r	N	D × 10^{-5} (cm^2/s)
(*N*-tert-butylacrylamide–co-*N*-vinylpyrrolidone) zinc oxide hydrogel	0.6841	1.00	500	121	10.01	3.80

In this study, loaded hydrogel also represented a smart-release behavior in different pH, shown in Fig 7. The loading efficiency of the drug was 54%. The higher loading efficiency could be achieved by improving the loading technique.

Protein Loading and Release

BSA molecules are negatively charged in phosphate buffer. As a result, there could be a strong electrostatic force of attraction between the hydrogel and BSA (Fig. 8). The porosity helped the migration of BSA. It facilitated loading by absorption, thereby increasing the surface area.

Free Radical Scavenging Activity of Hydrogel

The IC_{50} value was 96 µg for standard/control solution, shown in Fig. 9(a). The hydrogel's scavenging activity is expressed as a percentage in comparison to the antioxidant activity of these standard values refer to Table 9. The IC_{50} value indicates the amount of a substance needed to reduce a specific biological or chemical activity by 50%. Free radical scavenging assays measure an antioxidant's effectiveness in neutralizing free radicals. The IC_{50} value of 96 µg for a standard solution means that 96 µg is required to achieve a 50%

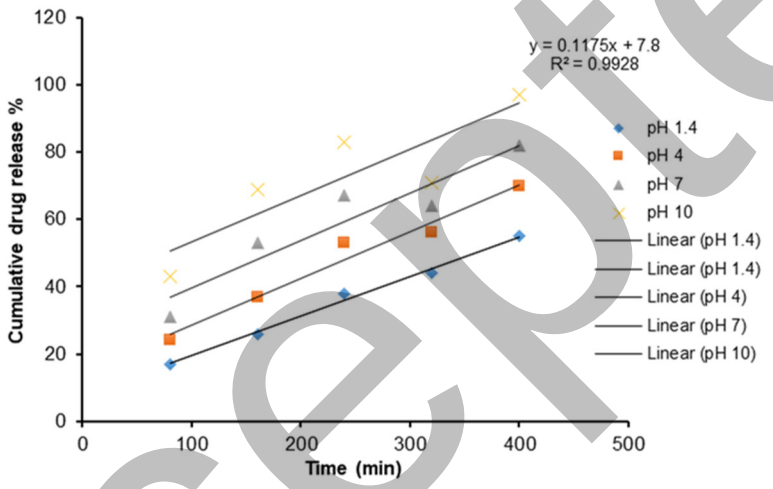

Fig 7. Cumulative drug release% behavior of (*N*-tert-butylacrylamide-co-*N*-vinylpyrrolidone) zinc oxide hydrogel cross-linked by MBA with time at different pH

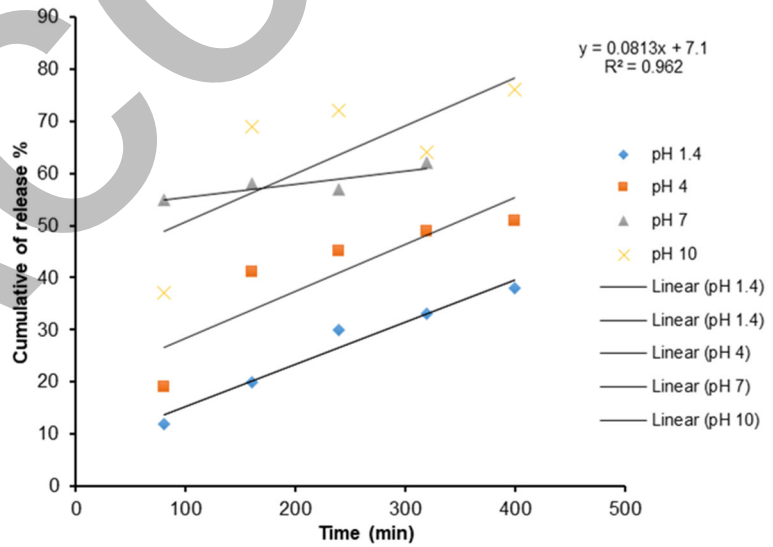

Fig 8. Cumulative protein release % behavior of (*N*-tert-butylacrylamide-co-*N*-vinylpyrrolidone) zinc oxide hydrogel cross-linked by MBA with time at different pH

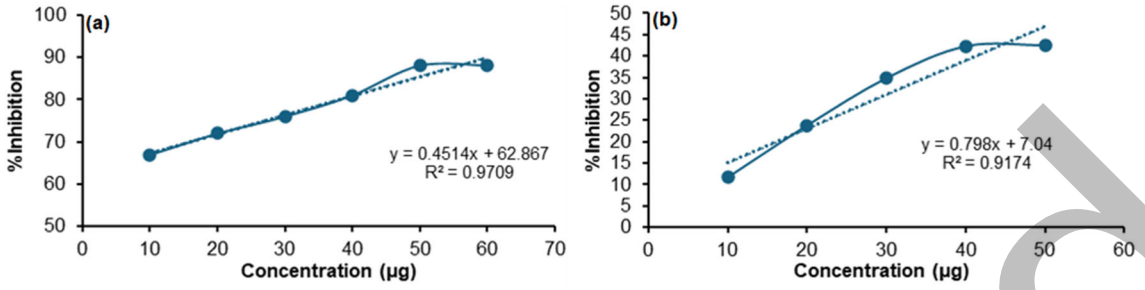

Fig 9. Graphical representation of %Inhibition of (a) standard solution and (b) (*N*-tertiary butyl acrylamide-co-*N*-vinylpyrrolidone) zinc oxide hydrogel

Table 9. Antioxidant activity of standard solution

Concentration (µL)	DPPH (mL)		OD	% Inhibition
10	3		0.346	67
20	3		0.287	72
30	3	Incubated in dark for 24 h	0.234	76
40	3		0.182	81
50	3		0.112	88
60	3		0.110	88

reduction in free radical activity. This value was used as a benchmark to compare the antioxidant capacities of synthesized hydrogels. A lower IC_{50} value signifies higher antioxidant potency, indicating that less substance is needed to achieve the same level of free radical scavenging.

The IC_{50} value was 53.8 µg for (*N*-tert-butylacrylamide-co-*N*-vinylpyrrolidone) zinc oxide hydrogel, shown in Fig. 9(b). The IC_{50} value of 53.8 µg for the (*N*-tert-butylacrylamide-co-*N*-vinylpyrrolidone) zinc oxide hydrogel indicates that 53.8 µg of this hydrogel is needed to achieve a 50% reduction in free radical activity [12]. This value reflects the hydrogel's antioxidant effectiveness: a lower IC_{50} signifies that the hydrogel is more efficient at neutralizing free radicals. Therefore, the lower IC_{50} value of 53.8 µg demonstrates that the hydrogel has a strong antioxidant capability, requiring less material to produce a significant scavenging effect compared to substances with higher IC_{50} values [12]. The antioxidant activities are summarized in Table 10.

Table 10. Antioxidant activity of (*N*-tert-butylacrylamide–co-*N*-vinylpyrrolidone) zinc oxide hydrogel

Concentration (µL)	DPPH (mL)		OD	%Inhibition
10	3		0.883	11.7
20	3	Incubated in dark for 24 h	0.762	23.8
30	3		0.652	34.8
40	3		0.578	42.2
50	3		0.576	42.4

Table 11. Evaluation of antimicrobial activity by standard agar well-diffusion method

No.	Organism	Type	Zone of inhibition (mm)		
			SP1	SP2	SP3
1	Bacteria	*Eschericia coli*	11.0	15.0	No zone
		αDH5	10.0	13.0	No zone
2	Fungi	*Trichophyton rubrum*	5.2	9.1	No zone

Antimicrobial Analysis

An antimicrobial study was conducted using the standard agar well diffusion method. The sensitivity of the antimicrobial activity was noted, and a heavier bacterial growth was inhibited at relatively low concentrations and was found to be in the demarcating line of the inhibition zone [20]. The solvent control was DMSO. The data are summarized in Table 11.

■ CONCLUSION

The results reveal that (*N*-tert-butylacrylamide–co-*N*-vinylpyrrolidone) zinc oxide hydrogel demonstrated significant antioxidant activity, highlighting the potential of the synthesized hydrogel as an effective healing agent for mitigating aging and anxiety-related degenerative diseases. Microbial growth was effectively inhibited with inhibition zones ranging from 10 to 15 mm. Fungal growth was also reduced at these concentrations, with inhibition zones of 5.2 to 9.1 mm. The reactivity ratios r_1 and r_2 were both 1, indicating ideal conditions for polymerization. The hydrogel's structural and reactivity properties are essential for designing an effective delivery system for targeted applications. By optimizing the monomer ratios, the hydrogel's efficiency and release behavior could be enhanced. It functions as a drug carrier, offering reduced toxicity and degradation, and has the potential for reactive targeting. Overall, the hydrogel was water-soluble, non-toxic, and antioxidant, ensuring its safety throughout the drug delivery.

■ ACKNOWLEDGMENTS

I would like to extend my deepest gratitude to Bharathiar University, Coimbatore, for providing the essential resources and facilities that made this research possible.

■ CONFLICT OF INTEREST

The authors declare that there are no conflicts of interest related to the publication of this article.

■ AUTHOR CONTRIBUTIONS

Pazhanisamy Periasamy: Conceptualize and design the work. Krithika Ramesh: analysis and interpretation of data, drafting and revising the manuscript. Jeyanthi Ponnusamy: manuscript revision and data interpretation.

■ REFERENCES

[1] Bhandari, K.P., Sapkota, D.R., Jamarkattel, M.K., Stillion, Q., and Collins, R.W., 2023, Zinc oxide nanoparticles—Solution-based synthesis and characterizations, *Nanomaterials*, 13 (11), 1795.

[2] Ashtaputrey, P., and Ashtaputrey, S., 2018, Study of swelling behavior and determination of swelling parameters of spherical hydrogels in water, *J. Drug Delivery Ther.*, 8 (4), 218–222.

[3] Shah, T.V., and Vasava, D.V., 2019, A glimpse of biodegradable polymers and their biomedical applications, *e-Polym.*, 19, 385–410.

[4] Kanmaz, N., Saloglu, D., and Hizal, J., 2019, Humic acid embedded chitosan/poly (vinyl alcohol) pH-sensitive hydrogel: Synthesis, characterization, swelling kinetic and diffusion coefficient, *Chem. Eng. Commun.*, 206 (9), 1168–1180.

[5] Sringam, J., Pankongadisak, P., Trongsatitkul, T., and Suppakarn, N., 2022, Improving mechanical properties of starch-based hydrogels using double network strategy, *Polymers*, 14 (17), 3552.

[6] Fenton, O.S., Olafson, K.N., Pillai, P.S., Mitchell, M.J., and Langer, R., 2018, Advances in biomaterials for drug delivery, *Adv. Mater.*, 30 (29), 1705328.

[7] Ibrahim, K.E., Bakhiet, A.O., Khan, A., and Khan, H.A., 2018, Recent trends in biomedical applications of nanomaterials, *Biosci., Biotechnol. Res. Asia*, 15 (2), 253–243.

[8] Khansary, M.A., 2016, Vapor pressure and Flory-Huggins interaction parameters in binary polymeric solutions, *Korean J. Chem. Eng.*, 33 (4), 1402–1407.

[9] Ni, S., 2017, Nanoparticles carrying natural product for drug delivery, *J. Drug Delivery Ther.*, 7 (3), 73–75.

[10] van der Sman, R.G.M., 2015, Biopolymer gel swelling analysed with scaling laws and Flory–Rehner theory, *Food Hydrocolloids*, 48, 94–101.

[11] Sen, M., Yakar, A., and Güven, O., 1999, Determination of average molecular weight between cross-links (Mc) from swelling behaviours of diprotic acid-containing hydrogels, *Polymer*, 40 (1), 2969–2974.

[12] Alidoust, S., Zamani, M., and Jabbari, M., 2021, Adsorption of free radical TEMPO onto Al_2O_3 nanoparticles and evaluation of radical scavenging activity, *Free Radical Res.*, 55 (9-10), 937–949.

[13] Autzen, A.A.A., Beuermann, S., Drache, M., Fellows, C.M., Harrisson, S., van Herk, A.M., Hutchinson, R.A., Kajiwara, A., Keddie, D.J., Klumperman, B., Russell, G.T., 2024, IUPAC recommended experimental methods and data evaluation procedures for the determination of radical copolymerization reactivity ratios from composition data, *Polym. Chem.*, 15 (18), 1851–1861.

[14] Koiry, B.P., and Singha, N.K., 2014, Copper-mediated controlled radical copolymerization of styrene and 2-ethylhexyl acrylate and determination of their reactivity ratios, *Front. Chem.*, 2, 91.

[15] Contreras-López, D., Saldívar-Guerra, E., and Luna-Bárcenas, G., 2013, Copolymerization of isoprene with polar vinyl monomers: Reactivity ratios, characterization and thermal properties, *Eur. Polym. J.*, 49 (7), 1760–1772.

[16] Yu, H., and Xing, P., 2022, Moisture absorption characterization of carbon fiber-reinforced polymer using Fickian and non-Fickian models, *Polym. Compos.*, 43 (12), 8935–8946.

[17] Zhokh, A., and Strizhak, P., 2019, Crossover between Fickian and non-Fickian diffusion in a system with hierarchy, *Microporous Mesoporous Mater.*, 282, 22–28.

[18] Mianehro, A., 2022, Electrospun bioscaffold based on cellulose acetate and dendrimer-modified cellulose nanocrystals for controlled drug release, *Carbohydr. Polym. Technol. Appl.*, 9, 100187.

[19] Gilarska, A., Lewandowska-Łańcucka, J., Horak, W., and Nowakowska, M., 2018, Collagen/chitosan/hyaluronic acid–based injectable hydrogels for tissue engineering applications: Design, physicochemical, and biological characterization, *Colloids Surf., B*, 170, 152–162.

[20] Salari, S., Bahabadi, S.E., Samzadeh-Kermani, A., and Yosefzaei, F., 2019, *In-vitro* evaluation of antioxidant and antibacterial potential of green synthesized silver nanoparticles using *Prosopis farcta* fruit extract, *Iran. J. Pharm. Res.*, 18 (1), 430–455.

[21] Liu, S., Li, X., and Han, L., 2022, Recent developments in stimuli-responsive hydrogels for biomedical applications, *Biosurf. Biotribol.*, 8 (4), 290–306.

[22] Jiang, B., Larson, J.C., Drapala, P.W., Pérez-Luna, V.H., Kang-Mieler, J.J., and Brey, E.M., 2012, Investigation of lysine acrylate containing poly(*N*-isopropylacrylamide) hydrogels as wound dressings in normal and infected wounds, *J. Biomed. Mater. Res., Part B,* 100B (3), 668–676.

[23] Luo, Y., Kirker, K.R., and Prestwich, G.D., 2000, Cross-linked hyaluronic acid hydrogel films: New biomaterials for drug delivery, *J. Controlled Release*, 69 (1), 169–179.

[24] Thippeswamy, M., Puttagiddappa, M.G., Thippaiah, D., and Satyanarayan, N.D., 2021, Poly(acrylamide-co-acrylic acid) synthesized, moxifloxacin drug-loaded hydrogel: Characterization and evaluation studies, *J. Appl. Pharm. Sci.*, 11 (2), 74–81.

[25] Naeem, F., Khan, S., Jalil, A., Ranjha, N.M., Riaz, A., Haider, M.S., Sarwar, S., Saher, F., and Afzal, S., 2017, pH responsive cross-link polymeric matrices based on natural polymers: Effect of process variables on swelling characterization and drug delivery properties, *BioImpacts*, 7 (3), 177–192.